Proceedings of the ASME 2012 Conference on Smart Materials, Adaptive Structures and Intelligent Systems
SMASIS2012
September 19-21, 2012, Stone Mountain, Georgia, USA

SMASIS2012-8254

THERMOMECHANICAL BEHAVIOR OF LOW CTE METAL-MATRIX COMPOSITES FABRICATED THROUGH ULTRASONIC ADDITIVE MANUFACTURING

Ryan Hahnlen
Smart Materials and Structures Lab
Dept. of Mechanical and Aerospace Engineering
The Ohio State University
Columbus, Ohio 43210
Email: hahnlen.1@osu.edu

Marcelo J. Dapino*
Smart Materials and Structures Lab
Dept. of Mechanical and Aerospace Engineering
The Ohio State University
Columbus, Ohio 43210
Email: dapino.1@osu.edu

ABSTRACT

Shape memory and superelastic NiTi are often utilized for their large strain recovery and actuation properties. The objective of this research is to utilize the stresses generated by prestrained NiTi as it is heated in order to tailor the CTE of metal-matrix composites. The composites studied consist of an Al 3003-H18 matrix with embedded NiTi ribbons fabricated through an emerging rapid prototyping process called Ultrasonic Additive Manufacturing (UAM). The thermally-induced strain of the composites is characterized and results show that the two key parameters in adjusting the effective CTE are the NiTi volume fraction and prestrain of the embedded NiTi. From the observed behavior, a constitutive composite model is developed based constitutive SMA models and strain matching composite models. Additional composites were fabricated to characterize the NiTi-Al interface through EDS and DSC. These methods were used to investigate the possibility of metallurgical bonding between the ribbon and matrix and determine interface shear strength. Interface investigation indicates that mechanical coupling is accomplished primarily through friction and the shear strength of the interface is 7.28 MPa. Finally, using the developed model, a composite was designed and fabricated to achieve a near zero CTE. The model suggests that the finished composite will have a zero CTE at a temperature of 135°C.

*Address all correspondence to this author.

INTRODUCTION

Shape Memory Alloys (SMAs) have unique properties due to a stress and temperature-dependent phase transformation between martensite, the low-temperature/high-stress phase, and austenite, the high-temperature/low-stress phase. While this transformation is most widely utilized for actuation purposes via the shape memory effect and high strain components through the superelastic response of initially austenitic alloys, this research utilizes the phase-dependent modulus of SMAs and their ability to generate transformation stresses when they are heated in an initially prestrained state. By embedding SMA elements within a metal-matrix composite, changes in elastic modulus allow for variable matrix reinforcement while transformation stresses can create axial loads, both of which are utilized to create unique thermally-induced strain responses. An SMA metal-matrix composite can be designed such that the stress that develops due to phase transformation and strain recovery can be utilized to offset the Coefficient of Thermal Expansion (CTE) of the matrix.

Composites in this research are fabricated using Ultrasonic Additive Manufacturing (UAM), a rapid prototyping technology based on ultrasonic metal welding. In ultrasonic metal welding, two workpieces are held together under a compressive load and ultrasonically vibrated relative to one another. The motion creates a friction-like action that disrupts surface oxides and shears surface asperities on a micro-scale creating nascent surfaces [1, 2]. The compressive load applied to the pieces causes opposing clean metal surfaces to form metallic bonds, thus join-

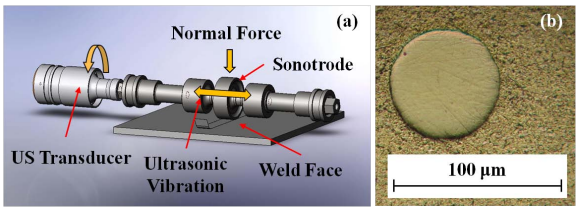

FIGURE 1. (a) IN THE UAM PROCESS, SUCCESSIVE LAYERS OF METAL TAPE ARE BONDED TOGETHER TO CREATE METAL COMPOSITES WITH SEAMLESSLY EMBEDDED MATERIALS AND FEATURES; (b) CROSS SECTION OF AN NiTi-Al COMPOSITE WITH 76 μm DIAMETER NiTi WIRE.

ing the two components. During UAM consolidation, illustrated in Figure 1 (a), the ultrasonic vibrations are generated by piezoelectric transducers and transmitted to the workpieces through tuned waveguides and a rolling sonotrode which is specially textured to grip the top workpiece. The primary benefit of UAM is the low process temperatures. Pieces are consolidated at room temperature and macro-scale heating results in temperatures below 195°C [3].

UAM makes it possible to embed thermally-sensitive materials such as SMAs, electroactive PVDF, fiber optics, and electronic components within a metal-matrix [4–7] which would not be possible with other metal-matrix composite technologies that require melting or high temperature diffusion for fabrication. During the welding phase, the ultrasonic vibrations of the workpieces and compressive stresses cause plastic deformation of the matrix material. The result is plastic flow of the matrix material around the embedded objects, creating close contact, mechanical interlocking, and possibly solid-state bonding between the composite components. To date, fibers ranging from 76 μm to 381 μm in diameter, Figure 1 (b), and ribbons up to 762 μm wide have been successfully embedded via UAM [3, 8, 9].

The key to tailoring thermally-induced strain with SMAs is to prestrain the embedded elements prior to embedding, transforming the twinned martensitic phase to detwinned martensite. When constrained and heated in the detwinned martensite phase, SMAs generate a tensile recovery stress, or blocking stress, that is nearly proportional to temperature [10–12]. During this heating cycle, as long as the SMA is perfectly constrained and does not under go plastic deformation, it will remain in its original detwinned martensitic phase. Creating metal-matrix composites with prestrained SMAs can be challenging as traditional methods such as casting or diffusion based processes have high temperature periods where the surrounding matrix will not provide constraint against the transforming and recovering SMA elements. Being a low temperature process, UAM is uniquely suited for creating SMA metal-matrix composites as the low temperature prevents transformation and subsequent recovery of the applied prestrain.

Due to the difference in CTE of the Al matrix and NiTi elements as well as blocking stresses generated by the embedded SMA, the fiber-matrix interface is subject to temperature dependent stresses. The nature of the interface between the matrix and embedded SMA elements in UAM remains a critical issue in designing and modeling smart UAM composites. If the interface fails to maintain the constraint on the SMA elements, the initial prestrain in the composite will be recovered upon heating, thus irrevocably changing the unique thermomechanical behavior of the composite.

In this paper, the thermally-induced strain of NiTi-Al UAM composites is examined to develop a constitutive model of the composite system. The interface between the NiTi and Al components of UAM composites is also investigated through Energy Dispersive X-ray Spectroscopy (EDS) and Differential Scanning Calorimetry (DSC) for use in determining the nature of the NiTi-Al coupling and strength of the interface. Lastly, using the composite model, a thermally-invariant composite is designed and fabricated.

EXPERIMENTAL PROCEDURE

Sample Fabrication

Three initial UAM composites were created to observe the thermomechanical behavior of NiTi-Al UAM systems. In these composites, the NiTi ribbons were heated in an unconstrained state to transform them to austenite and allowed to cool to form twinned martensite. While these composites were not expected to display constrained NiTi behaviors, they were created to characterize the thermo-elastic behavior of the composites. In fabricating the composites, two 152 μm thick Al 3003-H18 tapes were first consolidated on an Al 3003-H18 base plate. Rectangular NiTi ribbons, 254 μm by 762 μm, were placed on top of the second tape surface and clamped into position. Two additional Al tapes were consolidated over top of the ribbons to complete the UAM build. The composites were next machined to final dimensions and the base plates removed from the underside of the composites. Composites 1, 2, and 3 have NiTi volume fractions of 5%, 15%, and 20%, respectively.

Two additional composites were created in a similar manner with detwinned NiTi ribbons. The fabrication procedure for composites 4 and 5 is identical to that of 1-3, however then NiTi ribbons were fully detwinned by applying dead weight resulting in a tensile stress of 186 MPa, three times greater than the observed critical finish stress of this alloy at room temperature. Composite 4 was sectioned and polished for EDS analysis to study the NiTi-Al interface while composite 5 was machined to create a 15% NiTi composite and subsequently cut into three samples for DSC testing to observe the strength of the NiTi-Al interface. In both cases, the composites were cut to length using a lubricated low speed diamond precision saw to avoid heating and transformation of the NiTi ribbon at the cutting plane.

Thermomechanical Testing

For composites 1-3, thermally-induced strain was measured by heating the composites in a thermal chamber with an Al 3003-H18 reference sample for three cycles from 25 °C to 100 °C. During thermal cycles, the strain of each composite was measured with a strain gage matched to aluminum alloys and the temperature of the composites was monitored with a thermocouple placed next to the strain gages.

Since the CTE of the reference sample is known, the strain signal from the reference sample was used to remove the thermal dependency of the strain gages from the composite strain signals. To determine the composite strain response, the strain measured from the reference sample was subtracted from the strain measured from each composite and then the calculated thermal strain of the reference sample was added to the composite strain measurements [13]:

$$\varepsilon_{comp} = \varepsilon_{sig/comp} - \varepsilon_{sig/ref} + \alpha_{ref} \times \Delta T. \quad (1)$$

Here, $\varepsilon_{sig/comp}$ is the non-compensated strain signal from the composite, $\varepsilon_{sig/ref}$ is the strain signal from the reference sample, α_{ref} is the CTE of the reference material (23.2 $\mu\varepsilon/^{\circ}$C [14]), and ΔT is the change in temperature.

Interface Investigation

The polished section of NiTi-Al composite 4 was analyzed via EDS to observe composition across the NiTi-Al interface. EDS line scans were conducted at the top and bottom interfaces between the NiTi ribbon and Al matrix, shown in Figure 2, the most likely sites for metallic bonding between the composite components. If bonding between NiTi and Al does occur during the UAM process, two key observations are expected. First, for metallic bonding to occur, the oxide layers of both workpieces must be removed. Second, diffusion also occurs with metallic bonding and thus, elements from the matrix and embedded SMA, namely Ni, Ti, and Al, are expected to migrate across the interface if such bonding is present. In the conducted line scans, the atomic percentage of Al, Ni, Ti, and O were recorded at each point in the scan and plotted as a function of distance from the interface.

In preparation for DSC analysis, each sample from composite 5 was placed in an Al test pan and a single empty test pan was used as a comparative reference for all measurements. Using DSC analysis, the transformation of NiTi can be observed by measuring the difference in power needed to heat the test pan with the sample and the empty reference pan to the same temperature. The martensite to austenite (M-A) transformation for NiTi is endothermic and results in a well defined negative region termed an "endothermic peak" [15–17]. Since the embedded NiTi ribbon in composite 5 is highly prestrained, the M-A transformation must be accompanied by a 6% strain recovery. The surrounding Al matrix is unable to accomodate a 6% contraction without plastic yielding or failure of the interface. As such, by noting the temperature at which the endothermic peak occurs, a failure temperature can be measured and used in conjunction with the NiTi-Al composite models to determine the strength of the NiTi-Al interface.

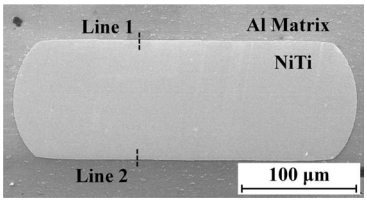

FIGURE 2. SEM IMAGE OF NiTi-Al COMPOSITE 4 SHOWING LOCATIONS OF LINES FOR EDS ANALYSIS.

For each sample, two heating cycles were recorded during DSC measurement. Temperature was increased at a rate of 10°C/sec to 200°C for the first cycle of each sample and up to 120°C for the second cycle in anticipation of lower transformation temperatures. Cooling was augmented by compressed air between cycles but was not recorded.

RESULTS AND DISCUSSION

Thermomechanical Testing

The temperature versus strain plots of composites 1-3 are shown in Figure 3 (a)-(c). For clarity, only the repeatable cycles, 2 and 3, are shown as the initial cycle is different than subsequent stable cycles. This initial behavior is believed to be due to a minute amount of residual detwinning and initial mechanical loading of the SMA elements from composite manufacturing. Similar effects have been observed in thermal cycling of constrained SMAs [10, 11]. An in-depth analysis of this initial, non-repeatable behavior has been discussed in previous work [3].

All three composites exhibit two linear regions corresponding to the martensite and austenite phases of the embedded NiTi ribbons. The difference between the slopes of the two linear regions is small in composite 1, however, the effect becomes more pronounced as NiTi volume fraction increases as displayed in the behaviors of composites 2 and 3. Since NiTi has a lower CTE than the Al matrix, the inclusion of NiTi elements will reduce the total composite CTE, α_{comp}, to varying degrees based upon the fiber volume fraction and phase dependent modulus [18–20]:

$$\alpha_{comp} = \frac{(1-\nu)(E_{Al})(\alpha_{Al}) + \nu(E_{NiTi})(\alpha_{NiTi})}{(1-\nu)(E_{Al}) + \nu(E_{NiTi})}. \quad (2)$$

Here, ν is the NiTi fiber volume fraction of the composite, E_{Al},

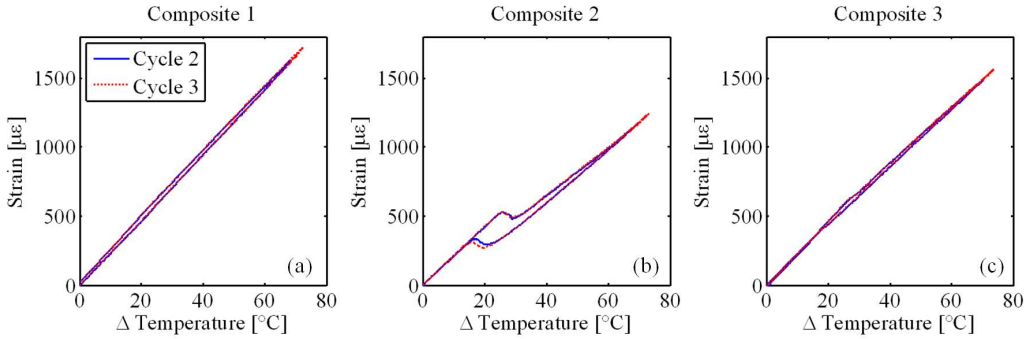

FIGURE 3. TEMPERATURE VERSUS STRAIN PLOTS FOR THE SECOND AND THIRD THERMAL CYCLES OF NiTi-Al: (a) COMPOSITE 1; (b) COMPOSITE 2; (c) COMPOSITE 3.

E_{NiTi}, α_{Al}, and α_{NiTi} are the elastic moduli and CTEs of Al and NiTi, respectively. At high temperatures, the modulus of the embedded NiTi increases, due to transformation to austenite, thus reducing the total composite CTE. This results in a higher strain-temperature slope at low temperatures and a lower slope at high temperatures corresponding to the higher and lower composite CTEs.

Composite 2 has an additional behavior unique among composites 1-3. Starting at approximately 50°C ($\Delta T = 25$°C) a negative strain-temperature slope is observed resulting in a contraction until approximately 55°C ($\Delta T = 30$°C) whereupon the composite resumes a linear strain-temperature relationship. On cooling, the recovered strain is introduced back into the composite over a temperature range of approximately 50°C to 40°C ($\Delta T = 25$°C to 15°C). This hysteretic behavior and strain recovery are characteristic of the shape memory effect of NiTi. While composites 1-3 were fabricated with twinned martensitic NiTi ribbons, this behavior indicates that the ribbons in composite 2 are partially detwinned. This is likely an effect of the rolling action of the UAM sonotrode applying tensile stresses along the ribbons during the embedding process. The unique behavior of composite 2 illustrates the significant effect detwinning of the embedded SMA elements can impart on the total composite response.

Composite Modeling

To model the thermal strain response of the composites, a strain matching method, similar to models used for SMA-epoxy composites [21–23], was employed. Under the condition that the interface remains intact, the strain in the fiber direction is identical for the Al matrix and NiTi ribbons. Further, the Al and NiTi strains can be expanded into their constituent components for mechanical, thermal, and transformation strain, as applicable:

$$\varepsilon_{Al} = \frac{1}{E_{Al}}\left(\Delta\sigma_{Al}\right) + \alpha_{Al}\left(\Delta T\right) \tag{3}$$

and

$$\varepsilon_{NiTi} = \frac{1}{E_{NiTi}}\left(\Delta\sigma_{NiTi}\right) + \alpha_{NiTi}\left(\Delta T\right) + \varepsilon_L\left(\xi_s - \xi_{so}\right), \tag{4}$$

where $\Delta\sigma$ is the change in total stress from the initial state, ξ_s is the stress-induced martensitic volume fraction, ξ_{so} is the initial stress-induced martensitic volume fraction, and ε_L is the maximum recoverable strain of NiTi.

In the thermally-induced strain tests, no external load is applied; the composite is allowed to freely expand or contract as the temperature changes. As such, a force balance is used to obtain the stress in the Al matrix in terms of NiTi stress:

$$\begin{aligned} \sigma_{NiTi}A_{NiTi} + \sigma_{Al}A_{Al} &= 0 \\ \sigma_{Al} &= -\frac{A_{NiTi}}{A_{Al}}\sigma_{NiTi} \\ \sigma_{Al} &= \frac{-\nu}{(1-\nu)}\sigma_{NiTi}, \end{aligned} \tag{5}$$

where A_{NiTi} and A_{Al} are the cross sectional areas of the NiTi ribbons and Al matrix, respectively. The variable change from cross sectional area to fiber volume fraction can be made because the NiTi ribbons provide long-fiber reinforcement of the Al matrix and the lengths of both components are equal, $L_{NiTi} = L_{Al}$. Assuming zero initial stress, the stress in the ribbons can be obtained as a function of temperature, material properties, volume fraction, and NiTi transformation terms by substituting (5) into (3), equating to (4), and solving for σ_{NiTi}:

$$\sigma_{NiTi} = \frac{\left(\alpha_{Al} - \alpha_{NiTi}\right)\left(\Delta T\right)}{\frac{1}{E_{NiTi}} + \frac{1}{E_{Al}}\frac{\nu}{(1-\nu)}} - \frac{\varepsilon_L\left(\xi_s - \xi_{so}\right)}{\frac{1}{E_{NiTi}} + \frac{1}{E_{Al}}\frac{\nu}{(1-\nu)}}. \tag{6}$$

This equation has two components: the first is the thermo-elastic component which any composite exhibits if a CTE mismatch

exists between the fibers and matrix; the second is due to the transformation-induced strain recovery of NiTi if it is embedded in a detwinned state ($\xi_{so} \neq 0$). If the embedded NiTi elements are not prestrained before fabrication, only the thermo-elastic stress component remains but is non-linear due to the change in modulus as the NiTi ribbons transform between martensite and austenite. Once the NiTi stress is calculated it can be used in (4) to determine total composite strain:

$$\varepsilon_{comp} = \frac{1}{E_{NiTi}} \left[\frac{(\alpha_{Al} - \alpha_{NiTi})(\Delta T)}{\frac{1}{E_{NiTi}} + \frac{1}{E_{Al}} \frac{\nu}{(1-\nu)}} - \frac{\varepsilon_L (\xi_s - \xi_{so})}{\frac{1}{E_{NiTi}} + \frac{1}{E_{Al}} \frac{\nu}{(1-\nu)}} \right] + \alpha_{NiTi}(\Delta T) + \varepsilon_L (\xi_s - \xi_{so}). \quad (7)$$

The same result is obtained by calculating the Al stress and using it in (3).

Composites 1-3 were assumed to be consolidated in a twinned martensite state, having an initial stress-induced volume fraction of zero. As such, the initial models for thermally-induced strain do not include the transformation strain recovery components and (7) becomes:

$$\varepsilon_{comp} = \frac{1}{E_{NiTi}} \left[\frac{(\alpha_{Al} - \alpha_{NiTi})(\Delta T)}{\frac{1}{E_{NiTi}} + \frac{1}{E_{Al}} \frac{\nu}{(1-\nu)}} \right] + \alpha_{NiTi}(\Delta T). \quad (8)$$

The strain calculation is completed by finding the elastic modulus of the NiTi ribbons as a function of martensitic volume fraction and the Al matrix as a function of temperature. The elastic modulus of the Al matrix is varied linearly using modulus values at different temperatures as found in the literature [14]. The elastic modulus of NiTi is found through a rule of mixtures between its martensite and austenite phases:

$$E_{NiTi} = E_A + \xi (E_M - E_A) \quad (9)$$

where E_A and E_M are the elastic moduli of austenite and martensite, respectively, and ξ is the total martensitic volume fraction. The martensitic volume fraction only decreases over the range defined by the austenite start and finish temperatures as composite temperature increases. Conversely, increasing volume faction only occurs over the martensitic start and finish temperatures while the composite temperature is decreasing. For the NiTi ribbons used in this study, the transition temperatures were found through electrical resistance tests and DSC and are shown in Table 1 with other experimentally derived material properties. Even in the thermo-elastic case, the increasing NiTi stress due to thermal mismatch of the NiTi ribbons and Al matrix necessitates using the stress-modified transformation temperatures which are assumed to vary linearly with stress [24–27]. In the case of an initial stress-induced martensitic volume fraction ($\xi_{so} \neq 0$) the transformation temperatures will increase further due to additional stresses generated from SMA strain recovery.

The martensitic volume fractions are found through equations based upon the Brinson [24] and Liang and Rogers [25,26] constitutive SMA models. For the M-A transformation the volume fraction is:

$$\xi = \frac{\xi_o}{2} \left(\cos \left[a_A (T - A_s^\sigma) \right] + 1 \right), \quad (10)$$

where

$$a_A = \frac{\pi}{A_f - A_s} \quad (11)$$

and

$$A_s^\sigma = A_s + \sigma_{NiTi}/C_A \quad (12)$$

where C_A is the stress influence coefficient for austenite transition temperatures. For the austenite to martensite (A-M) transformation the total volume fraction is calculated using:

$$\xi = \frac{1 - \xi_o}{2} \cos \left[a_M \left(T - M_f^\sigma \right) \right] + \frac{1 + \xi_o}{2}, \quad (13)$$

where

$$a_M = \frac{\pi}{M_s - M_f} \quad (14)$$

and

$$M_f^\sigma = M_f + \sigma_{NiTi}/C_M \quad (15)$$

where C_M is the stress influence coefficient for the martensitic temperatures and is assumed to be equal to C_A [27].

The thermo-elastic strains were modeled for each composite using the material properties found in Table 1. The model output can be seen for composites 1-3 in Figure 4 (a)-(c), respectively. For composites 1 and 3 the strain model closely matches the strain observed in the experiments, including unique high and low temperature linear regions and a small amount of hysteresis. However, the model does not describe the negative strain-temperature regions observed in composite 2. This confirms that

TABLE 1. MATERIAL PROPERTIES USED FOR COMPOSITE MODEL. UNLESS CITED, VALUES WERE FOUND EXPERIMENTALLY.

Property	Description	Value
E_A [28]	Austenite modulus	83 GPa
E_M	Martensite modulus	17.9 GPa
$E_{Al}(24\,^\circ\text{C})$ [14]	Al 3003 modulus, 24°C	68.3 GPa
$E_{Al}(100\,^\circ\text{C})$ [14]	Al 3003 modulus, 100°C	65.5 GPa
α_{Al} [14]	Al 3003 CTE	23.2 $\mu\varepsilon/^\circ$C
α_{NiTi} [27]	NiTi CTE	10 $\mu\varepsilon/^\circ$C
M_f	Martensite finish temp.	40°C
M_s	Martensite start temp.	45°C
A_s	Austenite start temp.	45°C
A_f	Austenite finish temp.	50°C
C_M, C_A	Stress influence coefficient	8.1 MPa
ε_L	Maximum recovery strain	-6%

the zero prestrain assumption is not valid when considering composite 2 and there is residual prestrain that was induced by the rolling action of the sonotrode during fabrication. The amount of prestrain and subsequent stress-induced martensite is determined by observing the amount of strain recovered as the NiTi ribbons go through the M-A transformation.

The strain recovery region observed in composite 2 is consistent over multiple cycles. Because of this, the transformation is assumed to recover and induce a repeatable amount of stress-induced martensite as the composite is heated and cooled. To this end, an assumption is made that $\xi_s = \xi_{so} \times \xi$ where ξ is found from (10) and (13) for purposes of calculating composite strain. By taking the average strain of the rising and falling high temperature linear regions at T=65°C, a temperature slightly beyond the M-A transformation region, and subtracting the modeled thermo-elastic strain for composite 2 at 65°C, the total composite recovery strain, $\varepsilon_{NiTi/X}$, is estimated to be 200 $\mu\varepsilon$. To calculate the initial stress-induced volume fraction from the total observed strain recovery, the thermo-elastic strain component from (8) is subtracted from the total strain from (7),

$$\varepsilon_{NiTi/X} = \frac{1}{E_{NiTi}}\left(\sigma_{NiTi/X}\right) + \varepsilon_L\left(\xi_s - \xi_{so}\right), \tag{16}$$

where $\sigma_{NiTi/X}$ is equal to the second term of (6). Considering $E_{NiTi} = E_A$ and $\xi_s = 0$ when the M-A transformation is complete,

$$\begin{aligned}\varepsilon_{NiTi/X} =& \frac{1}{E_{NiTi}}\left[\frac{-\varepsilon_L\left(\xi_s - \xi_{so}\right)}{\frac{1}{E_{NiTi}} + \frac{1}{E_{Al}}\frac{\nu}{(1-\nu)}}\right] + \varepsilon_L\left(\xi_s - \xi_{so}\right) \\ =& -\varepsilon_L\xi_{so}\left[1 - \frac{1}{1 + \frac{E_A}{E_{Al}}\frac{\nu}{(1-\nu)}}\right].\end{aligned} \tag{17}$$

Using 200 $\mu\varepsilon$ for $\varepsilon_{NiTi/X}$, the initial stress-induced martensitic volume fraction is found to be 1.9%. Using (7) with the calculated value for ξ_{so}, the red dashed line in Figure 4 (b) shows the thermally-induced strain model for composite 2 including the transformation strain component. With the inclusion of the transformation strain term, the model closely matches the experimental data and exhibits the expanded hysteretic region originally observed.

Interface Investigation

The change in atomic percent of elemental composition of EDS lines 1 and 2 are shown in Figure 5. While EDS line scan points were taken at intervals of ~1 μm, the resolution of the measurement is also dependent upon the electron interaction radii of the material being scanned. A Monte Carlo simulation of electron flight paths estimated interaction radii for Al and NiTi of 2.6 μm and 1.2 μm, respectively. The result of the interaction radii is that the EDS results will show a transition equal to the sum of the radii, 3.8 μm, as a scan transitions from a perfect, diffusionless interface between an Al and NiTi system. In considering the EDS results, a transition region greater than 3.8 μm will indicate the presence of diffusion while a transition less than or equal to 3.8 μm will indicate that there is no measurable diffusion between the materials.

Line scan 1 shows the Al to NiTi transition occurring over 3.0 μm while line 2 has a transition of 3.3 μm, both of which are below the threshold for measurable diffusion indicating that there is no diffusion based bonding between the NiTi and Al constituents. Further, in both line scans there is a peak in oxygen content as the Al and NiTi composition lines intersect. This indicates that at least one oxide layer is still present at the interface. A key aspect to bonding via UAM is the removal of surface oxide at the interface of the workpieces. From the EDS results, the ultrasonic vibrations generated for the consolidation process were not sufficient to create nascent surfaces at the NiTi-Al interface, thus making a metallurgical bond unlikely. While metallurgical bonding between NiTi and Al is doubtful, the SEM image in Figure 2 shows very close contact around the entire perimeter of the NiTi ribbon cross section. This indicates that the load transfer necessary for the behaviors observed in the CTE testing is accomplished through a friction dominated interface.

Results from the DSC measurements are shown in Figure 6. Only the plots from samples 2 are shown, though the behavior

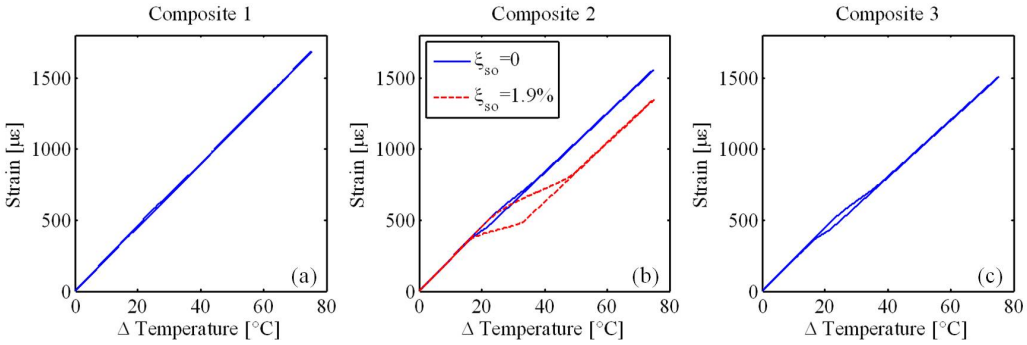

FIGURE 4. THERMALLY-INDUCED STRAIN MODELS FOR NiTi-Al: (a) COMPOSITE 1; (b) COMPOSITE 2; (c) COMPOSITE 3.

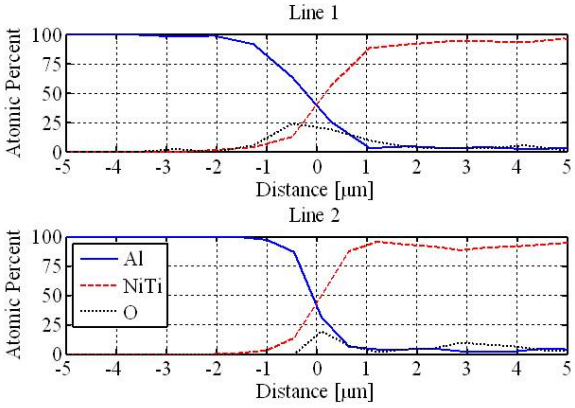

FIGURE 5. EDS LINE SCAN RESULTS OF NiTi-Al COMPOSITE 4.

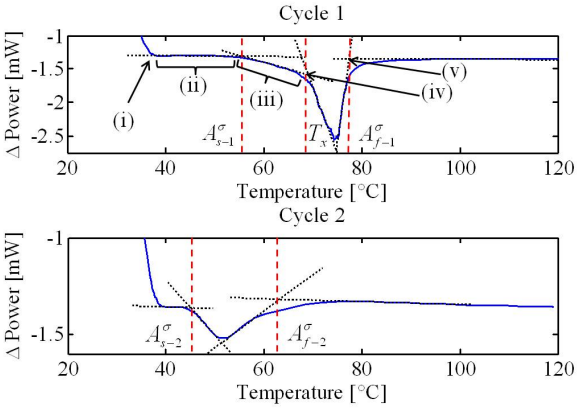

FIGURE 6. DSC HEATING CYCLES 1 AND 2 OF NiTi-Al COMPOSITE 5.

for all samples are similar. The endothermic peaks observed in both cycles indicate the M-A transformation temperature range of the embedded NiTi ribbons and display the change in temperatures between the first and second cycles. Five key regions of interest are identified in the first cycle and are defined by either consistent behavior or transition points between areas of different behavior. Region (i) is the initial state and is characterized by the stabilization of the differential power measurement from the DSC system. Region (ii) is characterized by a nearly horizontal power versus temperature relationship. Region (iii) is defined by the a negative power-temperature slope prior to the endothermic transformation peak. Region (iv) is noted by the transition between region (iii) and the low temperature portion of the endothermic peak at temperature T_x. Region (v) is the intersection of linear interpolations of the high temperature portion of the endothermic transformation peak and the consistent behavior at higher temperature characterized by an approximately horizontal power versus temperature curve.

An interpretation of the composite behavior at each region is shown in Figure 7. At region (i), the composite is considered to be in a reference state to which all other regions are compared. Through region (ii), linear thermal expansion of the total composite is occurring. In region (iii), the temperature has surpassed the composite austenite start temperature, A^{σ}_{s-1}. As the composite temperature increases, the NiTi ribbon generates recovery stress which is resolved as a compressive stress on the Al matrix. The result is an apparent reduction in CTE of the composite in this region due to the combined thermal and mechanical loading. At region (iv) the generated stresses overcome the shear strength of the NiTi-Al interface and transformation of the detwinned martensite continues unrestrained. As the NiTi ribbons transform they recover the induced prestrain, contracting within the Al matrix while, simultaneously, the Al matrix is able to freely expand as governed by its CTE. At region (v) the NiTi transformation and strain recovery is complete. Further heating results in linear thermal expansion of the composite. It is noted that while the NiTi ribbon has contracted within the Al matrix, there is still friction between the ribbon and matrix which allows load transfer and will govern thermomechanical properties of the composite. Region (vi) is cooling of the composite. During cool-

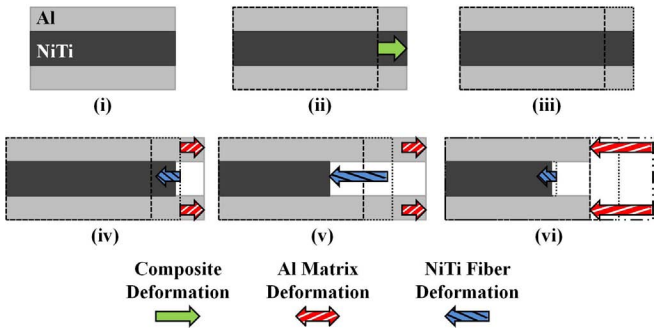

FIGURE 7. REPRESENTATION OF REGIONS IDENTIFIED IN DSC CURVE: (i) REFERENCE STATE; (ii) LINEAR THERMAL EXPANSION OF TOTAL COMPOSITE; (iii) REDUCED/SUPPRESSED EXPANSION DUE TO GENERATION OF BLOCKING STRESSES; (iv) ONSET OF NiTi-Al INTERFACE FAILURE; (v) NiTi TRANSFORMATION COMPLETE; (vi) COOL TO REFERENCE TEMPERATURE (NOT PLOTTED).

ing and in subsequent cycles, the samples will behave similar to composites 1 and 3 due to the new zero prestrain condition and thermally-induced strain can be described by (8).

Using the intersection of linear interpolations of different identified regions, several important temperatures are determined. The intersection of regions (ii) and (iii) is taken as the initial austenite start temperatures, A^{σ}_{s-1}, as previously noted. This is different than the austenite start temperature of the ribbon, A_s, due to the thermo-elastic stresses generated by the different CTEs of the Al and NiTi components, thereby increasing the transformation temperatures as a function of temperature. In a similar manner, the initial austenite finish temperature, denoted A^{σ}_{f-1}, is different than the austenite finish temperature of the material, A_f, however in this case it is due to generated blocking stresses in addition to the thermo-elastic stresses. The temperature at region (iv) is denoted T_x and represents the onset of the NiTi-Al interface failure.

The second thermal cycle in Figure 7 shows the shift in the endothermic peak and transformation temperatures, A^{σ}_{s-2} and A^{σ}_{f-2}. The austenite start temperature of cycle 2 is lower than that of cycle 1 indicating that there was a persistent preload on the NiTi ribbon after embedding. This preload is likely due to a combination of tension developed during the clamping process and the rolling action of the sonotrode imparting a tensile load during embedding similar to the load in composite 2 that created the stress-induced martensitic volume fraction. A^{σ}_{f-2} is significantly lower than A^{σ}_{f-1} due to the absence of blocking stresses generated during heating above A^{σ}_{s-2}. Further, cycle 2 does not exhibit a temperature range analogous to region (iii) in which blocking stresses were generated in the initial cycle. This is supporting evidence that all prestrain was recovered in the first cycle due to failure of the interface. The temperatures of interest for all 3 samples are given in Table 2.

TABLE 2. TRANSITION AND FAILURE TEMPERATURES FOR COMPOSITE 5 SAMPLES 1, 2, AND 3.

Temperature [°C]	Sample 1	Sample 2	Sample 3
A^{σ}_{s-1}	55.5	55.5	56.4
A^{σ}_{f-1}	77.7	77.4	77.5
A^{σ}_{s-2}	44.5	45.0	44.7
A^{σ}_{f-2}	62.6	63.2	60.0
T_x	69.2	69.0	68.4

The NiTi stress in the DSC samples was calculated using (6) assuming an initial stress induced volume fraction of 1. At the average failure temperature of 68.9°C, stress in the NiTi due to thermo-elastic and recovery stresses is 174 MPa. Using the average tensile stress at failure, the ultimate shear strength at the interface was calculated:

$$\tau_f = \sigma_x \frac{A_{NiTi}}{A_{shear}} \tag{18}$$

where σ_x is the NiTi stress at failure, A_{NiTi} is the ribbon cross sectional area, and A_{shear} is the interface surface area. The average shear stress at failure is found to be 7.28 MPa. While the recovery stress generated by the NiTi is not dependent upon ribbon length, the interface surface area is proportional to the length of ribbon embedded within the matrix. This implies that as composite length increases for similar NiTi-Al composites, so will the shear area, reducing shear stress and increasing failure temperature, eventually reaching a point where composite failure may occur through yielding of the NiTi elements, compressive yielding of the Al matrix, or buckling of the composite rather than interfacial failure.

Thermally-Invariant Composite

Utilizing the same procedure as used for composites 1-5, an additional composite was made with two 254 μm by 762 μm NiTi ribbons embedded at the midplane of the composite. Prior to embedding, the ribbons were detwinned by applying a dead weight, similar to the ribbons used in composite 5. The final composite is to be machined to have a NiTi volume fraction of 15%, similar to composite 2, however, due to the fully detwinned NiTi ribbons, the behavior of the new composite is expected to be substantially different.

Using the developed model, Figure 8 shows the predicted thermally-induced strain of composite 6. In heating the composite, prior to A^{σ}_{s}, the strain will be governed by linear thermal expansion, however at temperatures higher than A^{σ}_{s}, the recovery stresses are expected to nearly eliminate any strain in the

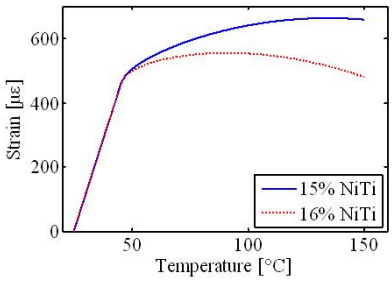

FIGURE 8. MODELED TEMPERATURE VERSUS STRAIN RESPONSE OF NiTi-Al COMPOSITE 6 COMPARING EFFECT OF NiTi FIBER VOLUME FRACTION.

composite due to additional thermal expansion. The increasing blocking stresses completely offset the thermal expansion of the composite at a temperature of 135°C, after which the effective composite CTE becomes negative. It is noted that this behavior can be further tailored in future composites by selecting an SMA with lower transformation temperatures to reduce the linear CTE prior to the generation of blocking stresses and also by increasing the SMA fiber volume fraction to adjust the shape of the blocking force curve. The effect of volume fraction is demonstrated in Figure 8. While the composite as designed will achieve a zero CTE at 135°C, increasing the NiTi fiber volume fraction by 1% causes the zero CTE to be realized at 91°C with further heating causing the composite to under go relative contraction with increasing temperature.

CONCLUDING REMARKS

In this research we have developed unique metal-matrix composites consisting of an Al matrix and shape memory NiTi ribbons. Composites were the subject of experimental characterization to determine their thermomechanical behavior and the nature of the NiTi-Al interface to construct an accurate composite model and ultimately create a thermally-invariant NiTi-Al composite structure.

Investigation of the thermomechanical behavior focused on the thermally-induced strain. It was found that while fiber volume fraction creates an increasingly variable bi-linear effect as the embedded NiTi undergoes the M-A transformation, the prestrain level of the embedded NiTi ribbons creates larger changes in the thermomechanical behavior and even allows for regions of negative CTE. The observed thermally-induced strain behavior was used to develop a model combining elements from strain matching composite models with thermodynamically based constitutive SMA models. The resulting model closely matches the thermally-induced strain behaviors observed for composites 1-3.

The interface between the NiTi ribbons and Al matrix has also been characterized through EDS and DSC. Using EDS, no evidence of diffusion or metallurgical bonding was observed, indicating that the primary mechanism of load transfer between NiTi and Al is friction. Through DSC analysis, a failure temperature of small composite samples consisting of 15% highly prestrained NiTi by volume was obtained and used to determined the ultimate shear strength of the NiTi-Al interface, 7.28 MPa. While the blocking force of the NiTi ribbons is not dependent upon fiber length, the shear stress at the interface is, indicating that beyond a critical fiber length the interface is not a likely source of composite failure.

Based upon the behaviors observed and the model predictions, an additional composite was fabricated. This composite consists of 15% NiTi by volume which has been fully detwinned prior to embedding. The model predicts that above the A_s^σ temperature, the composite will have a drastically reduced effective CTE and ultimately a CTE equal to zero at 135°C. Continuing work is focused on charcterizing the latest composite and developing new composites using SMAs with lower transition temperatures to attain zero CTE behavior near room temperature.

ACKNOWLEDGMENT

The authors would like to acknowledge Mark Norfolk and Karl Graff from the Edison Welding Institute for their assistance and use of UAM equipment as well as Phillip Evans from MIT Lincoln Laboratory. The NiTi ribbon was provided by Nitinol Devices and Components. Financial support for this research was provided by the member organizations of the Smart Vehicle Concepts Center (www.SmartVehicleCenter.org), a National Science Foundation Industry/University Cooperative Research Center (I/UCRC). R.H. was partially supported by a Smart Vehicle Concepts Graduate Fellowship.

REFERENCES

[1] De Vries, E., 2004. "Mechanics and mechanisms of ultrasonic metal welding". PhD thesis, The Ohio State University, Columbus, OH.

[2] Graff, K., 2005. *New Developments in Advanced Welding*. Woodhead Publishing Limited.

[3] Hahnlen, R., and Dapino, M., 2011. "Performance and modeling of active metal-matrix composites manufactured by ultrasonic additive manufacturing". Proc. SPIE 7979.

[4] Siggard, E., 2007. "Investigative research into the structural embedding of electrical and mechanical systems using ultrasonic consolidation". Master's thesis, Utah State University, Logan, UT.

[5] Kong, C., and Soar, R., 2005. "Fabrication of metal-matrix composites and adaptive composites using ultrasonic consolidation process". *Materials Science and Engineering A, **412***, pp. 12–18.

[6] Kong, C., Soar, R., and Dickens, P., 2004. "Ultrasonic consolidation for embedding SMA fibres within aluminium matrices". *Composite Structures,* ***66***, pp. 421–427.

[7] Masurtschak, S., and Harris, R. A., 2010. "Enabling techniques for secure fibre positioning in ultrasonic consolidation for the production of smart material structures". Proc. SPIE 7981.

[8] Hahnlen, R., and Dapino, M., 2010. "Active metal-matrix composites with embedded smart materials by ultrasonic additive manufacturing". Proc. SPIE 7645.

[9] Hahnlen, R., Dapino, M., Short, M., and Graff, K., 2009. "Aluminum-matrix composites with embedded Ni-Ti wires by ultrasonic consolidation". Proc. SPIE 7290.

[10] Vokoun, D., Kafka, V., and Hu, C., 2003. "Recovery stresses generated by NiTi shape memory wires under different constrain conditions". *Smart Materials and Structures,* ***12***, pp. 680–685.

[11] Tsoi, K. A., Schrooten, J., Zheng, Y., and Stalmans, R., 2004. "Part I. thermomechanical characteristics of shape memory alloys". *Materials Science and Engineering A,* ***368***, pp. 286–298.

[12] Zak, A. J., Cartmell, M. P., Ostachowicz, W. M., and Wiercigroch, M., 2003. "One-dimensional shape memory alloy models for use with reinforced composite structures". *Smart Materials and Structures,* ***12***, pp. 338–346.

[13] Lanza di Scalea, F., 1998. "Measurement of thermal expansion coefficients of composites using strain gauges". *Experimental Mechanics,* ***328***(4), pp. 233–241.

[14] Kaufman, J., ed., 1999. *Properties of Aluminum Alloys: Tensile, Creep, and Fatigue Data at High and Low Temperatures*. The Aluminum Association, Inc. and ASM International.

[15] Zheng, Y. J., Schrooten, J., Tsoi, K. A., and Sittner, P., 2003. "Qualitative and quantitative evaluation of the interface in activated shape memory alloy composites". *Experimental Mechanics,* ***43***(2), pp. 194–200.

[16] Zheng, Y. J., Schrooten, J., Tsoi, K. A., and Stalmans, R., 2002. "Thermal response of glass fiber/epoxy composites with embedded TiNiCu alloy wires". *Materials Science and Engineering A,* ***335***, pp. 157–163.

[17] Zheng, Y. J., Cui, L. S., and Schrooten, J., 2005. "Basic design guidelines for SMA/epoxy smart composites". *Materials Science and Engineering A,* ***390***, pp. 139–143.

[18] Clyne, T., and Withers, P., 1993. *An Introduction to Metal Matrix Composites*. Cambridge University Press.

[19] Staab, G., 1999. *Laminar Composites*. Butterworth-Heinemann.

[20] Schapery, R. A., 1968. "Thermal expansion coefficients of composite materials based on energy principles". *Journal of Composite Materials,* ***2***(3), pp. 380–404.

[21] Sittner, P., Michaud, V., and Schrooten, J., 2002. "Modeling and material design of SMA polymer composites". *Materials Transactions,* ***43***(5), pp. 984–993.

[22] Sittner, P., and Stalmans, R., 2000. "Developing hybrid polymer composites with embedded shape-memory alloy wires". *JOM,* ***52***(10), pp. 15–20.

[23] Sittner, P., Stalmans, R., and Tokuda, M., 2000. "An algorithm for prediction of the hysteretic responses of shape memory alloys". *Smart Materials and Structures,* ***9***(4), pp. 452–465.

[24] Brinson, L., 1993. "One dimensional constitutive behavior of shape memory alloys". *Journal of Intelligent Material Systems and Structures,* ***4***(2), pp. 229–242.

[25] Liang, C., and Rogers, C. A., 1990. "One-dimensional thermomechanical constitutive relations for shape memory materials". *Journal of Intelligent Material Systems and Structures,* ***1***, pp. 207–234.

[26] Liang, C., and Rogers, C. A., 1997. "One-dimensional thermomechanical constitutive relations for shape memory materials". *Journal of Intelligent Material Systems and Structures,* ***8***, pp. 285–302.

[27] Lagoudas, D., 2008. *Shape Memory Alloys*. Science and Business Media, LLC.

[28] Johnson Matthey, 2011. Nitinol technical specifications: Transformation, physical, electrical, magnetic and mechanical. Website: http://jmmedical.com.